

# Computational Model for Forced Expiration from Asymmetric Normal Lungs

ADAM G. POLAK<sup>1,2</sup> and KENNETH R. LUTCHEN<sup>1</sup>

<sup>1</sup>Department of Biomedical Engineering, Boston University, Boston, MA and <sup>2</sup>Chair of Electronic and Photonic Metrology, Wroclaw University of Technology, Wroclaw, Poland

(Received 18 June 2002; accepted 16 April 2003)

**Abstract**—We present a computational model to predict maximal expiration through a morphometry-based asymmetrical bronchial tree. A computational model with the Horsfield-like geometry of the airway structure, including wave-speed flow limitation and taking into consideration separate airflows from several independent alveolar compartments has been derived. The airflow values are calculated for quasistatic conditions by solving a system of nonlinear differential equations describing static pressure losses along the airway branches. Calculations done for succeeding lung volumes result in the semidynamic maximal expiratory flow–volume (MEFV) curve. Simulations performed show that the model captures the main phenomena observed *in vivo* during forced expiration: effort independence of the flow–volume curve for the most of vital capacity, independence of limited flow on the properties of airways downstream to the choke points, characteristic differences of lung regional pressures and volumes, and a shape of their variability during exhalation. Some new insights into the flow limitation mechanism were achieved. First, flow limitation begins at slightly different time instants in individual branches of the bronchial tree, however after a short period of time, all regional flows are limited in a parallel fashion. Hence, total flow at the mouth is limited for most of the expired lung volume. Second, each of the airway branches contribute their own flow–volume shape and just these individual flows constitute the measured MEFV curve. Third, central airway heterogeneity can play a crucial role in modification of the entire flow. Fourth, the bronchial tree asymmetry is responsible for a nongravitational component of regional volume variability. Finally, increased inhomogeneity yields results that cannot be explained nor re-created with the use of a symmetrical structure of the bronchial tree. © 2003 Biomedical Engineering Society.  
[DOI: 10.1114/1.1588651]

**Keywords**—Forced expiration, Bronchial tree asymmetry, Heterogeneous lung emptying, Regional flow interdependence.

## INTRODUCTION

It has been shown that lung heterogeneity plays an important role in respiratory system pathology and influences results of lung examinations. Experimental and

model studies on the respiratory system demonstrate that heterogeneous constriction of airways accompany asthma and can be a crucial determinant of hyper-responsiveness via an increase in lung impedance.<sup>2,18,19,30,48,54</sup> Administration of histamine or methacholine also produces heterogeneous constriction<sup>19,31,33,48</sup> and consequent inhomogeneity of ventilation.<sup>18,57,58</sup> Similarly, the heterogeneity of emphysema predestines patients to surgery and enables prediction of postoperative improvement in lung functioning.<sup>4,6,55</sup> Standard assessment of lung function in all these diseases relies heavily on spirometric indices derived from a maximum forced expiratory maneuver. Some researchers have concluded that maximal expiration curve is insensitive to inhomogeneous pattern of regional lung emptying.<sup>23,36,41,56</sup> We present the use of a morphometrically based model to advance our understanding of how inherent asymmetries in lung structure might influence such measures.

During forced expiration the driving pressure exceeds a critical level and the resulting airflow, due to the flow limiting mechanism, approaches an asymptotic value.<sup>15</sup> Since there exists a relationship between maximum expiratory flow and degree of lung inflation, flow has been plotted against lung volume establishing the maximum expiratory flow–volume (MEFV) curve.<sup>24</sup> This relationship is effort independent for a wide range of vital capacity, and its features are determined by respiratory system mechanical properties. More specifically, pathological combinations that increase airway resistance or alter airway wall and parenchymal properties can change the shape of the MEFV curve.

Several experimental works have examined the MEFV curves during nonuniform maximal emptying of the respiratory system, both on a rather simple structure<sup>64</sup> and excised or open-chest lungs.<sup>32,38,56,59,60</sup> In principal, the asymmetries can play an important role in constituting the shape of the flow–volume curve,<sup>29,34,36</sup> and a noticeable interest in this problem has been demonstrated.<sup>16,17,23,34</sup> Nevertheless, the question of how the heterogeneity of the lung structure influences the

Address correspondence to Kenneth R. Lutchén, PhD, Professor and Chairman, Biomedical Engineering, Boston University, 44 Cummington Street, Boston, MA 02215. Electronic mail: klutch@bu.edu

MEFV curve and spirometric indices still remains open. Specifically, which of the MEFV indices reflect the level of heterogeneity and what kind of a relationship exists between them? Also, how should the MEFV curve be processed to assess the level of lung inhomogeneity? In principle, one approach for addressing these issues is through mathematical modeling.

Several computational models have been offered to probe the mechanics governing the MEFV curve. These efforts range from including the wave-speed theory<sup>9,50</sup> to calculate the pressure drop in a single elastic airway, to the use of a symmetric Weibel's geometry of the bronchial tree<sup>61</sup> so as to distinguish pressure losses along the whole airways.<sup>12,14,28,40,42,51</sup> It is known, however, that lungs, especially diseased ones, do not empty uniformly. Alveolar pressures and segment airflows vary among distinct regions as lung volume decreases.<sup>29,32,36,59,60</sup> Bronchial structure asymmetry<sup>20,21</sup> seems to be the main source of this inhomogeneity in a healthy lung. Only a few approaches to model the maximum expiration from two different lung regions can be found in the literature.<sup>26,41,52</sup>

Here, we elaborate a computational model for predicting maximum expiratory flow in an asymmetric, morphometrically consistent lung model. We further examine how particular structural and mathematical assumptions influence local and total flow limitations. This model is the first step in concretely deciphering how MEFV curve shape and spirometric indices derive from a heterogeneously emptying asymmetric human lung. The scope of this paper is to present the computational model itself, its validation, as well as the influence of airway asymmetry and model form in case of a healthy lung. It is shown that the model captures the main phenomena observed during forced expiration as well as how the airway asymmetry influences the MEFV curve. Future studies will examine the impact of heterogeneous constriction akin to asthma and influence of inhomogeneity of emphysema distribution.

## THEORY

### *Preliminaries*

During simulation of forced expiration it has been common to assume that flow is quasi-static and one-dimensional but dependent on lung volume.<sup>12,14,28,40,42</sup> The main benefit is the reduction of dynamic relationships to static dependencies (for fast dynamics) and constants (for slow dynamics). For example, airway wall dynamics simplifies to the inclusion of area–transmural pressure relationship. Likewise, alveolar pressure is regarded as constant for a given lung volume. The airflow dynamics then translates to a flow dependent, nonlinear pressure drop along an elastic tube.

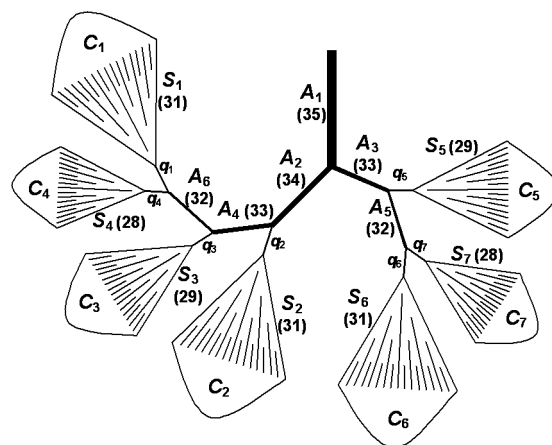


**FIGURE 1. Asymmetric structure of the bronchial tree: A, separate airways (numbers in parentheses denote Horsfield's orders); S, symmetric peripheral trees (numbers in parentheses denote Horsfield's orders of "mother" airways); C, alveolar compartments; and  $q$ , airflows from the compartments.**

In our model the asymmetric structure of the bronchial tree follows the approach of Horsfield.<sup>18,21</sup> The trachea is an extrathoracic airway and its dimensions do not depend on pleural pressure. All other airways are treated as intrapleural, and external pressure of the intrathoracic airways is assumed to be equal to the pleural pressure.<sup>14,28,42</sup> Calculations of flow in the junctions are made for the equal static pressures at the downstream ends of the daughter airways and upstream end of the mother one, neglecting convective accelerations in this region.<sup>52</sup> Thus, during a MEFV maneuver the bronchial tree can be seen as a bifurcating net of nonlinear, pressure and lung volume dependent resistors, driven by lung regional pressures and "grounded" through the upper airways to the atmosphere.

Full calculations for the entire asymmetric model are not yet practical and we must reduce calculation complexity while retaining fundamental features of the asymmetries in the airway tree. Hence, airway branching from the trachea follows the Horsfield asymmetry down to a designated order in the bronchial tree. Then, airways of smaller order than this are replaced with a symmetric structures which we call peripheral airway trees (Fig. 1; the 32nd order was chosen in most of simulations performed). The dimension of each peripheral tree depends on the order of the mother airway. Orders of the daughter airways are chosen in such a way that they always belong to the next Weibel generation (see Table 1). The peripheral trees are symmetric and they lead to identical alveoli of the same properties (volume, pressure, recoil). Hence, we can group all alveoli subtended by a given tree as a single alveolar compartment or region. The result is that the lungs are divided into a number of

**TABLE 1. Bronchial tree data: Horsfield's orders, Weibel's generations, Horsfield's recursion indexes indicating the degree of asymmetry, maximal lumen areas (at 3 kPa), lengths (at RV), and Lambert's coefficients for pressure-area curves ( $\alpha_0$ ,  $\alpha'_0$ ,  $n_1$ ,  $n_2$ ). Lambert's data extrapolated for generations 17 to 23.**

Horsfield's order	Weibel's generation	Horsfield's recursion index	$A_m$ (mm <sup>2</sup> )		$l_{RV}$ (mm)		$\alpha_0$	$\alpha'_0$ (1/kPa)	$n_1$	$n_2$
			Horsfield's	Weibel's	Horsfield's	Weibel's				
35	0	1	201	267	100	120	0.882	0.110	0.5	10
34	1	2	96.8	123	14.3	32.8	0.882	0.110	0.5	10
33	1	3	113	123	16.9	32.8	0.882	0.110	0.5	10
32	2	3	50.3	57.9	7.14	13.1	0.686	0.510	0.6	10
31	2	3	44.2	57.9	6.30	13.1	0.686	0.510	0.6	10
30	3	3	34.9	27.2	7.32	5.22	0.546	0.810	0.7	10
29	4	3	26.9	17.6	7.31	8.73	0.428	1.00	0.7	10
28	4	3	22.5	17.6	6.30	8.73	0.428	1.00	0.8	10
27	5	3	14.3	10.1	7.02	7.35	0.337	1.25	0.8	10
26	5	3	9.57	10.1	6.19	7.35	0.337	1.25	0.9	10
25	6	3	9.46	7.09	5.57	6.19	0.265	1.42	0.9	10
24	6	3	7.50	7.09	6.42	6.19	0.265	1.42	1.0	10
23	7	3	6.51	4.64	5.17	5.23	0.208	1.59	1.0	10
22	7	3	6.03	4.64	5.96	5.23	0.208	1.59	1.0	10
21	8	3	5.60	3.11	5.31	4.41	0.164	1.74	1.0	10
20	8	3	4.95	3.11	5.25	4.41	0.164	1.74	1.0	10
19	9	3	4.34	2.14	5.03	3.72	0.129	1.84	1.0	10
18	9	3	3.73	2.14	4.16	3.72	0.129	1.84	1.0	10
17	10	3	3.14	1.52	4.07	3.14	0.102	1.94	1.0	10
16	10	3	2.46	1.52	3.36	3.14	0.102	1.94	1.0	10
15	11	3	1.91	1.09	3.10	2.65	0.0800	2.06	1.0	9
14	11	2	1.43	1.09	2.74	2.65	0.0800	2.06	1.0	9
13	12	2	1.00	0.805	2.31	2.23	0.0630	2.18	1.0	8
12	12	1	0.709	0.805	2.03	2.23	0.0630	2.18	1.0	8
11	13	0	0.454	0.609	1.65	1.88	0.0490	2.26	1.0	8
10	14	0	0.312	0.475	0.714	1.59	0.0390	2.33	1.0	8
9	15	0	0.221	0.379	0.851	1.34	0.0310	2.39	1.0	7
8	16	0	0.181	0.310	0.682	1.13	0.0240	2.43	1.0	7
7	17	0	0.145	0.258	0.487	0.955	0.0200	2.55	1.0	7
6	18	0	0.126	0.222	0.383	0.804	0.0149	2.62	1.0	7
5	19	0	0.126	0.196	0.312	0.679	0.0118	2.69	1.0	6
4	20	0	0.126	0.177	0.312	0.573	0.00925	2.75	1.0	6
3	21	0	0.126	0.163	0.312	0.484	0.00728	2.80	1.0	6
2	22	0	0.126	0.155	0.312	0.408	0.00573	2.86	1.0	6
1	23	...	0.126	0.151	0.312	0.344	0.00451	2.91	1.0	6

independent alveolar regions, which can empty nonuniformly.

All calculations are made for time instants being increased by 0.01 s (i.e., flow sampling at 100 Hz), and then compartment volumes are being calculated by integration of flows (trapezoidal method). As mentioned, we assumed quasistatic conditions of flow. This means that during calculations related to a given time instant (or lung volume) flow is treated as steady, i.e., all derivatives on time that appear in dynamic equations are zero. However, in a succeeding time instant (or lung volume), new conditions (driving pressure, lung recoil) create a new flow value. In effect, a semidynamic expiration is simulated.

### Lung Pressures

Forced expiration is caused by recoil of lung tissue (given by the static recoil pressure,  $P_{st}$ ) and a combina-

tion of chest tissue recoil and expiratory muscle contraction (influencing the pleural pressure,  $P_{pl}$ ). Experimental data from Pardaens *et al.*<sup>40</sup> suggest that at the beginning of forced expiration  $P_{pl}$  increases in an exponential manner and, after reaching a maximal value, decreases linearly (or slightly exponentially). However, the exact knowledge of the pleural pressure is not necessary since during flow limitation airflow is effort independent, and thus does not depend on  $P_{pl}$  value for most of lung volumes. Alveolar pressure ( $P_A$ ) is a sum of static recoil and pleural pressures, so only two of them are independent. For convenience,  $P_A$  and  $P_{st}$  have been chosen in this study since they are used directly in calculations.

Previous investigations<sup>39</sup> have examined three phenomena potentially influencing alveolar pressure at the beginning of expiration: thorax inertia, compressibility of alveolar gas, and expiratory muscle force accretion. Simulations, based on a simple pneumatic model of the

respiratory system, showed that increase of the expiratory muscle force (and simultaneous relaxation of inspiratory ones) is the dominant process. According to experimental data of Agostoni and Fenn<sup>1</sup> and taking into account pressure drop on linear thorax tissue resistance ( $R_T$ ), the alveolar pressure dependence on lung volume ( $V_L$ ) can be proposed in the following form:<sup>3,42</sup>

$$P_A(V_L, t) = P_m(1 - e^{-t/\tau}) \left( \frac{V_L - RV}{VC} \right) - R_T Q = P_d, \quad (1)$$

where  $P_m$ -maximal expiratory pressure,  $\tau$  is time constant of expiratory muscle,  $RV$  is the residual volume,  $VC$  is the vital capacity, and  $Q$  is the flow measured at the mouth. Equation (1) is consistent with the published data.<sup>1,40,51</sup> The equation expresses a total effect of both expiratory muscle force and  $P_{st}$  (the first term), lessened by frictional dissipation of pressure in thorax tissues (the second term).

Referring all pressure values to the atmospheric one, the alveolar pressure becomes the driving pressure ( $P_d$ ) in forced expiration. During airflow the gravitational term of pressure is negligible and pressure lateral to airway walls ( $P$ ) equals the static component of the total pressure. In the alveoli there is no convective flow, and the alveolar lateral pressure is equal to  $P_A$ . Lateral pressure at the peripheral airways leading to the alveoli amounts also to  $P_A$  due to a huge number of bronchioli and negligible convective flow in this region. The static pressure just outside the mouth is zero (i.e., it is the atmospheric pressure). However, for some short distance in the air the stream of expired gas retains a dynamic component (equal to  $\frac{1}{2}\rho u^2$ , where  $\rho$  is gas density and  $u$  is gas velocity), which is approximately the same as the dynamic component of gas at the airway outlet. Consequently, the lateral pressure at the downstream end of upper airways is close to zero. Any difference that occurs between the lateral and atmospheric pressures is a small fraction of the pressure drop in the upper airways, takes place downstream to the flow limiting mechanism, and essentially will not influence the airflow. It follows that during forced expiration the driving pressure  $P_d$  is approximately equal to the lateral pressure drop along each pathway from the alveoli to the airway outlet, thus knowledge of its value is necessary to predict airflow.

Gas flow through an elastic tube, which acts as the Starling resistor, depends on the transmural pressure ( $P_{tm}$ ), i.e., the difference between the internal lateral pressure and the external pleural one. Since the alveolar pressure is a sum of the pleural and lung recoil pressures,<sup>14,28,40,42</sup> the transmural pressure at the given point  $x$  in a bronchus can be described:

$$P_{tm}(x) = P(x) - P_{pl} = [P_A - \Delta P_{lt}(x)] - P_{pl} \\ = P_{st}(V_L) - \Delta P_{lt}(x), \quad (2)$$

where  $\Delta P_{lt}$  is a lateral pressure drop between the alveoli and this point, and  $P_{st}$  is the static recoil pressure at volume  $V_L$ . A linear-exponential pressure-volume relation for the lung<sup>5</sup> has been used in this study. It consists of a linear section for smaller volumes and exponential part for higher volumes (as proposed by others<sup>7,49</sup>), fitted at the transition volume ( $V_{tr}$ ):

$$P_{st}(V_L) = \begin{cases} \frac{V_L - V_0}{C_E}, & V_L \leq V_{tr}, \\ \frac{V_m - V_{tr}}{C_E} \ln \left( \frac{V_m - V_{tr}}{V_m - V_L} \right) + \frac{V_{tr} - V_0}{C_E}, & V_L > V_{tr}, \end{cases} \quad (3)$$

where:  $V_m$ ,  $V_0$  are the maximal and minimal lung volumes,  $C_E$  is the lung compliance during expiration at zero recoil pressure, close to the compliance measured at the FRC. We use the linear-exponential characteristics since it is more general and better fits experimental data.<sup>5</sup> Particularly, our approach enables future studies on heterogeneous changes in regional  $P$ - $V$  relationships.

Since the lung tissue exhibits hysteresivity,<sup>13</sup> the expiratory part of the transpulmonary pressure-lung volume relationship should be used, especially as the forced expiration is a dynamic process.<sup>32</sup> It is additionally assumed that  $V_0 = RV$ .

#### Pressure Drop Along an Elastic Tube

Quasistatic flow in a collapsible bronchus is described by the tube law based on the cross-section area-transmural pressure relationship.<sup>9,11,50</sup> Viscous energy dissipation causes a decrease in static pressure followed by a decrease of lumen area. The effect of airway closing is augmented by kinetic acceleration of gas in a narrowed airway, producing additional drop of lateral pressure. When flow velocity approaches the wave speed of pressure disturbance propagation along the airway wall, the loss of lateral pressure is strongly amplified causing the airway to narrow much quicker than by frictional dissipation alone. This phenomenon has been described by Lambert *et al.*<sup>28</sup> using the conservation of momentum (static, incompressible flow case):

$$\frac{dP}{dx} = \frac{-f(x)}{1 - S^2(x)} = \frac{-f(x)}{1 - \frac{\rho q^2}{A^3(x)} \left( \frac{\partial A}{\partial P_{tm}} \right)}, \quad (4)$$

where  $dP/dx$  is the gradient of lateral pressure along the bronchus,  $f(x)$  is the elementary dissipative pressure loss

(pressure drop per unit distance) at the point  $x$ ,  $S = u/c$  is the local speed index equal to the ratio between flow ( $u$ ) and wave ( $c$ ) speed,  $q$  is the volume flow in the bronchus,  $A$  is the cross-sectional area, and  $\partial A/\partial P_{tm}$  is the elementary compliance of the airway wall (compliance per unit distance) dependent on  $P_{tm}$ . The relation for  $f(x)$  in a bifurcating airway system can be based on experimental studies of Reynolds and Lee.<sup>46,47</sup> They derived the empirical formula in case of multigeneration model:

$$f(x) = [a + bR_N(x)] \frac{8\pi\mu q}{A^2(x)}, \quad (5)$$

where the value of the elementary pressure drop depends on flow, the local Reynolds number ( $R_N$ ) and gas viscosity ( $\mu$ ). Scaling coefficients,  $a$  and  $b$ , were determined first for a canine bronchial cast<sup>47</sup> (3.4 and 0.0021, respectively), and then for a human one<sup>46</sup> (1.5 and 0.0035). The second case has been used in the present study. Another approach was applied by Collins *et al.*<sup>8</sup> They examined the pressure–flow relationship in a single bifurcation with the developed subtraction method and proposed the following description:

$$f(x) = \begin{cases} 8\pi\mu q A^{-2}(x), & R_N(x) < 55, \\ (a + b\sqrt{R_N(x)})8\pi\mu q A^{-2}(x), & R_N(x) \geq 55. \end{cases} \quad (6)$$

The values for  $a$  and  $b$  are 0.556 and 0.067, respectively.<sup>51</sup> The top part of Eq. (6) and the expression outside the brackets on the right side of Eq. (5) constitute the Poiseuille formulas for elementary viscous pressure drop during laminar flow. We will examine the impact of both forms of  $f(x)$ .

To calculate lateral pressure loss along the bronchus, one has to know dimensions and mechanical properties of the airway, the transmural pressure at the beginning of the bronchus (i.e., the lateral pressure loss between the alveoli and its inlet), the flow value  $q$ , and the airway's length. Intrapleural bronchi lengths  $l$  change with the cube root of lung volume  $V_L$ .<sup>14,22</sup>

$$l(V_L) = l_{RV} \left( \frac{V_t + V_L}{V_t + RV} \right)^{1/3}, \quad (7)$$

where  $l_{RV}$  is airway length at residual volume and  $V_t$  is lung tissue volume.

The pressure loss in the mouth  $\Delta P_U$  is estimated according to the experimentally derived formula<sup>25,40,45,62</sup> simplified to the following form:

$$\Delta P_U = R_U Q^r, \quad (8)$$

with the same values of coefficients  $R_U$  and  $r$  as used by Polak.<sup>42</sup>

### Difficulties with the Horsfield Structure

Simulation of forced expiration with the asymmetric model of the bronchial tree is computationally complex. First, the pressure drop along a single airway [Eq. (4)] cannot be computed simply by integration because the right-hand equation variables depend on the left-hand pressure loss between the beginning of the tube and the given point. Hence, we must employ the technique of numerical integration to solve this differential equation. Second, the right-hand function of Eq. (4) contains a singularity at  $q = A\sqrt{A/\rho(\partial P_{tm}/\partial A)}$ . Third, the pressure drop in each airway depends on the upstream airway properties that influence the pressure drop between the alveoli and its inlet as well as the downstream airways that determine flow  $q$  in the segment, and both phenomena are nonlinear. Finally, there are over 6 million airways in the asymmetric Horsfield model that may possess distinct features at any given time during the expiration. Solving such a problem is computationally unrealistic.

A reasonable simplification of the asymmetric bronchial tree structure is achieved by replacing peripheral parts of the Horsfield tree with symmetrical Weibel's ones. This decreases the number of unknowns in a system of equations which has to be solved while hastening the computation of pressure drop along the peripheral part. The latter occurs because there is only one unknown flow within the peripheral tree, and it is divided by bifurcations into subflows of the same value.

## ALGORITHM

### Scheme of Calculations

A flow chart of the algorithm is presented in Fig. 2. From the morphological data, a lung structure is created. This structure takes into account the airway order below which the symmetric trees appear (e.g., Fig. 1). Then starting values are ascribed to compartmental volumes  $V_C$  and flows  $q$ . Calculations are carried out with time increments  $\Delta t$  of 0.01 s. New values of compartmental volumes are computed by subtracting the portion of air ( $\Delta V = q\Delta t$ ) expired during the last period of the VC maneuver. The crucial point of the procedure is the assessment of pressure losses  $\Delta P$  in the airways, done by numerical integration of the differential equation (4). If flow limitation (FL) happens in any bronchi, all peripheral flows are being decreased until they are subcritical. Temporary values of pressure losses in the bronchial tree, driving pressures and compartmental flows are used to estimate flow increments needed to satisfy the set of Eqs. (9) given below. If flows do not exceed the local

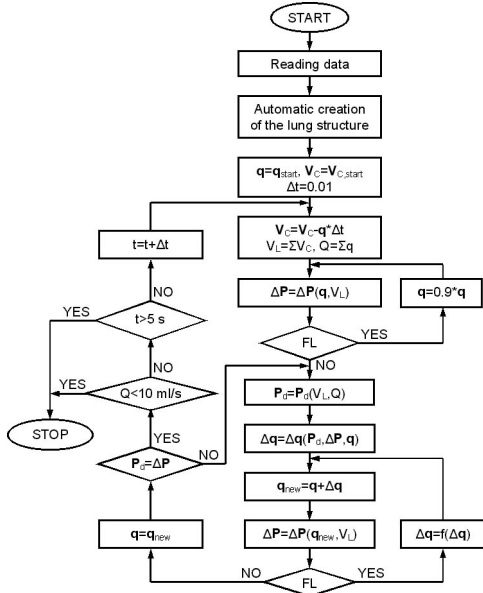


FIGURE 2. A flow chart of the algorithm for simulation of forced expiration:  $q$ , a vector of compartmental flows;  $V_C$ , a vector of compartmental volumes (the sum of starting  $V_C$  is equal to TLC);  $Q$ , airflow at the mouth opening;  $V_L$ , instant lung volume;  $\Delta P$ , a vector of calculated pressure drops along the bronchial branches;  $P_d$ , a vector of driving pressures at the bronchial branches; FL, flow limitation; and  $t$ , time of expiration. For a detailed description see the text.

wave speeds and the driving pressures are equal to the pressure losses along the bronchial branches, the algorithm goes forward the next time instant. Simulation ends when the total flow falls below 10 ml/s or expiration goes over 5 s. Algorithm parameters associated with numerical accuracy (e.g., tolerance of integration, threshold values of loop exits, or a time step) were carefully chosen to make numerical errors negligible. Details of the numerical procedures used are described in the Appendix.

#### Nonlinear System of Equations

The main task of this algorithm is to find the compartmental flows which will ensure that pressure drops along the bronchial branches are equal to the driving

pressures. Considering flows through the airways and static pressures at their connections in the Horsfield network (Fig. 1), one is able to write an equation for each pathway between an alveolar compartment and the mouth. Following Sud *et al.*,<sup>53</sup> we sum pressure losses  $\Delta P_i$  of the succeeding airways belonging to the given branch, and set this sum to the driving pressure  $P_{dk}$  of the  $k$ th lung compartment. These drops of pressure are computed according to Eq. (4), taking into account the actual lung volume (determining transmural pressure) and airflow, which is a sum of flows coming from the compartmental branches leading to the airway given. The approach above yields the following system of equations:

$$\sum_i \Delta P_i(q_1, q_2, \dots, q_k) = P_{d1},$$

$$\sum_j \Delta P_j(q_1, q_2, \dots, q_k) = P_{d2},$$

(9)

⋮

$$\sum_l \Delta P_l(q_1, q_2, \dots, q_k) = P_{dk}.$$

Solving this set of  $k$  nonlinear equations with  $k$  unknowns ( $q_1 - q_k$ ) allows determination of all segment flows and node pressures for the given time and lung volume in quasi-static conditions. A sum of peripheral flows  $q$  gives the expiratory flow measured in the mouth.

#### Pressures in Alveolar Compartments

Since alveoli are divided in the model into separate compartments, they may empty with different rates. It is assumed that compartment volume at the beginning of expiration is proportional to the number of alveoli served by the given peripheral tree. As a result of nonuniform emptying, different compartment volumes can exist at the same time, generating various recoil pressures. This phenomenon was modeled by the following modification of Eq. (3):

$$P_{st,k}(V_{Ck}) = \begin{cases} \frac{N_{alv}/N_{ak} \cdot V_{Ck} - V_0}{C_E}, & \frac{N_{alv}}{N_{ak}} V_{Ck} \leq V_{tr}, \\ \frac{V_m - V_{tr}}{C_E} \ln\left(\frac{V_m - V_{tr}}{V_m - N_{alv}/N_{ak} \cdot V_{Ck}}\right) + \frac{V_{tr} - V_0}{C_E}, & \frac{N_{alv}}{N_{ak}} V_{Ck} > V_{tr}, \end{cases} \quad (10)$$

where  $P_{st,k}$  is the recoil pressure in the  $k$ th compartment,  $V_{Ck}$  is the volume of the compartment,  $N_{alv}$  is the total number of alveoli, and  $N_{ak}$  is the number of alveoli in the given compartment. Consequently, the driving pressures for the pathways ( $P_{dk}$ ) are also changed [compare Eqs. (1) and (3)]:

$$P_{dk} = \begin{cases} P_m(1 - e^{-t/\tau}) \left( \frac{V_L - RV}{VC} \right) - R_T Q - \frac{V_L - N_{alv}/N_{ak} \cdot V_{Ck}}{C_E}, & \frac{N_{alv}}{N_{ak}} V_{Ck} \leq V_{tr}, \\ P_m(1 - e^{-t/\tau}) \left( \frac{V_L - RV}{VC} \right) - R_T Q - \frac{V_m - V_{tr}}{C_E} \ln \left( \frac{V_m - N_{alv}/N_{ak} \cdot V_{Ck}}{V_m - V_L} \right), & \frac{N_{alv}}{N_{ak}} V_{Ck} > V_{tr}. \end{cases} \quad (11)$$

According to the above innovation and Eq. (2), transmural pressure at the point  $x$  inside an airway is equal to the differences between recoil pressures of compartments generating flows coming to this airway and pressure drops between them and the point  $x$  (this scheme of calculations follows the bronchial tree structure shown in Fig. 1). Flows between compartments (i.e., penduluft-like conditions) are allowed.

### Data

Lambert's area-pressure curves apply to the airway generations<sup>28</sup> within the Weibel structure and need to be translated for use in our Horsfield based asymmetrical bronchial tree. The transformation has been based on Wiggs *et al.*<sup>63</sup> Here we assume that the given Horsfield order corresponds to the Weibel's generation with the largest number of airways of this order and no smaller than the previous one (Table 1). Maximal lumen areas ( $A_m$ ) are calculated from airway diameters at TLC (Ref. 21) and airway lengths at RV are rescaled from TLC values<sup>21</sup> using Eq. (7).

## SIMULATION STUDIES

We performed a series of simulation studies to examine how flow limitation and the level of inhomogeneity of flows and pressures are influenced by (a) lung asymmetry, (b) the form of mathematical formulas for pressure drop along an airway, and (c) the morphological data used to define the model structure.

With regard to probing the effects of asymmetry, the algorithm allows choosing the order of airways upstream of which the bronchial subtrees are substituted by symmetric structures. The smaller the order chosen, the bigger the level of lung asymmetry that is achieved. Simulations were done to check the effect of increasing asymmetry on MEFV curves, for the critical order values equal 35, 34, 33, 32, and 31.

With regard to inhomogeneity of flows and pressures, the alveoli in the model are grouped in a few distinct compartments of different volumes. Due to asymmetry of the bronchial tree, heterogeneous rates of airflows from the alveolar regions may be expected. Moreover, flow limitation may begin within separate bronchial tree branches, but at different total lung volumes. To observe expiratory flows from the alveolar regions and detect

moments when flow limitation begins (i.e., when flow starts to be independent on the driving pressure), simulations were performed for baseline conditions and for a 25% increase of the maximal expiratory pressure  $P_m$ .

In these simulations we also need to evaluate whether our model is consistent with the phenomenon of the interdependence of regional expiratory flows.<sup>32,38,52,56,59,64</sup> Hence, we tracked pressures and volumes of alveolar compartments during forced expiration simulation. Since the mechanical properties of parenchyma have been assumed to not vary between compartments, the only source of compartmental flow heterogeneity is asymmetry of the bronchial tree. Coefficients of variation (CV), i.e., ratios between standard deviations and mean values, were used as indexes of pressure and volume variability.

The mathematical formulas for pressure drop along an airway must determine the shape of the MEFV curve. To test the importance of this relationship, simulations have been performed with different descriptions of steady pressure–flow characteristics<sup>8,46,47</sup> [Eqs. (5) and (6)].

Finally, with regard to the morphological data used for defining model geometry, two of bronchial tree geometry models were considered: the symmetric structure described by Weibel<sup>61</sup> and the asymmetric one presented by Horsfield *et al.*<sup>21</sup> Although a transition between both of them can be proposed (Table 1), airways with corresponding Horsfield's orders and Weibel's generations will differ in dimensions. Since the forced vital capacity test is very sensitive to airway cross-sectional areas (and in minor extent to their lengths),<sup>27</sup> we investigated a shift in the MEFV curve produced by the change in bronchi morphology.

## RESULTS OF SIMULATIONS

Selection of the bronchial order below which the airways are replaced with the symmetric structures determines the level of lung asymmetry in the model. Figure 3 shows the MEFV curves achieved for increasing heterogeneity of lungs. Switching from order 35 (the trachea) to 34 actually caused a greater maximum flow. There after, however, asymmetries that extend to lower airway orders resulted in systematic decreases in airflow. The degree of flow reduction depends however on the

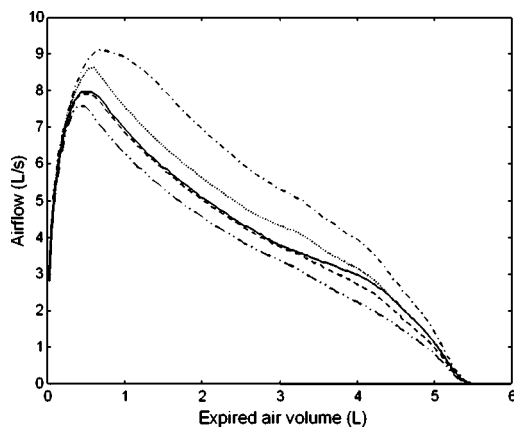


FIGURE 3. Influence of model asymmetry on the MEFV curve. Asymmetry given by the order of the smallest separate airway included in the model: 35th order (.....), 34th order (- · - · -), 33rd order (- - -), 32nd order (—), and 31st order (----).

stage of modification of the lung structure. Generally, development of bronchial tree asymmetry suppresses the air flow measured at the mouth outlet.

To evaluate how effort impacts local maximal flows we compared baseline simulations to simulations run after increasing the maximal expiratory pressure  $P_m$  by 25% (Fig. 4). It is apparent that a greater effort has the effect only on the very first part of expiration at which flow limitation has not yet occurred. After that, flows from compartments 1 and 6, 3 and 5, as well as 4 and 7 start to be similar. Additionally, flows from the compartments possessing greater number of alveoli (number 1, 2, and 6, compare Fig. 1) are larger.

The heterogeneity of lung emptying is reflected through the variability in compartment pressures and volumes as shown in Fig. 5 (the volumes have been normalized with respect to their initial values). Shapes of

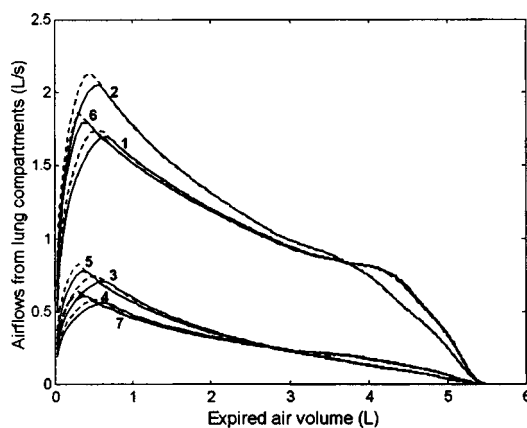


FIGURE 4. Heterogeneous airflows from lung compartments for normal (—) and 25% increased (---) maximal expiratory pressure  $P_m$ . Internal numbers indicate alveolar compartments (see Fig. 1).

alveolar pressure changes [Fig. 5(A)] are determined by Eq. (1). Small differences between these shapes result from the history of emptying of the individual regions. There is greater variety among the behavior of compartment volumes [Fig. 5(B)]. Some compartments empty faster at the beginning to slow down during the last period of expiration, whereas others behave in an opposite way. The variability among compartmental pressures (i.e., the coefficient of variation, CV) rapidly increases at the beginning of expiration to about 2.2% and then slowly decreases [Fig. 5(C)] and CV of compartmental volumes grows systematically up to 12% and drops off in the end of expiration [Fig. 5(D)].

Influence of the form of the equation describing pressure losses is demonstrated in Fig. 6. It has been shown that the smallest pressure drop in a bronchus of given dimensions (i.e., the smallest resistance) is achieved with the formula proposed by Collins *et al.*<sup>8</sup> This produces the higher airflow for every lung volume. Alternation of coefficient values in the Reynolds equation decreases the influence of the laminar factor and increases the impact of the turbulent one. This reduces flow during the first part of expiration and augments it at the end of the VC maneuver.

Comparison between expiratory curves calculated with Weibel's and Horsfield's data is shown in Fig. 7. It is apparent that applying the Horsfield data higher airflow is reached for every lung volume.

## DISCUSSION

We have presented, for the first time, a computational model for predicting maximum expiratory flow efforts in an asymmetric, morphometrically consistent lung model. The model predicts that the inherent asymmetry of the airway tree will distinctly influence the heterogeneity of flow-limitation during a forced expiratory maneuver.

### *Validity of the Model*

Our model assumes that flow is constant (its derivative on time equals to zero) for a given lung volume. This approach allows omitting the partial differential equations describing flow in a tube. Viscoelastic properties and inertia of airway walls are also neglected. Though some other authors used the same method,<sup>12,14,28,40,42</sup> Elad and co-workers incorporated dynamic equations in their simulations (omitting dynamics of airway walls).<sup>10,51</sup> They did this at the expense of reduction of the airway tree geometry to a one "trumpet" tube with physical properties varying continuously, as first proposed by Fry.<sup>14</sup> In this case airway asymmetry cannot be modeled. The quasi-steady flow approach has been chosen in our investigations.

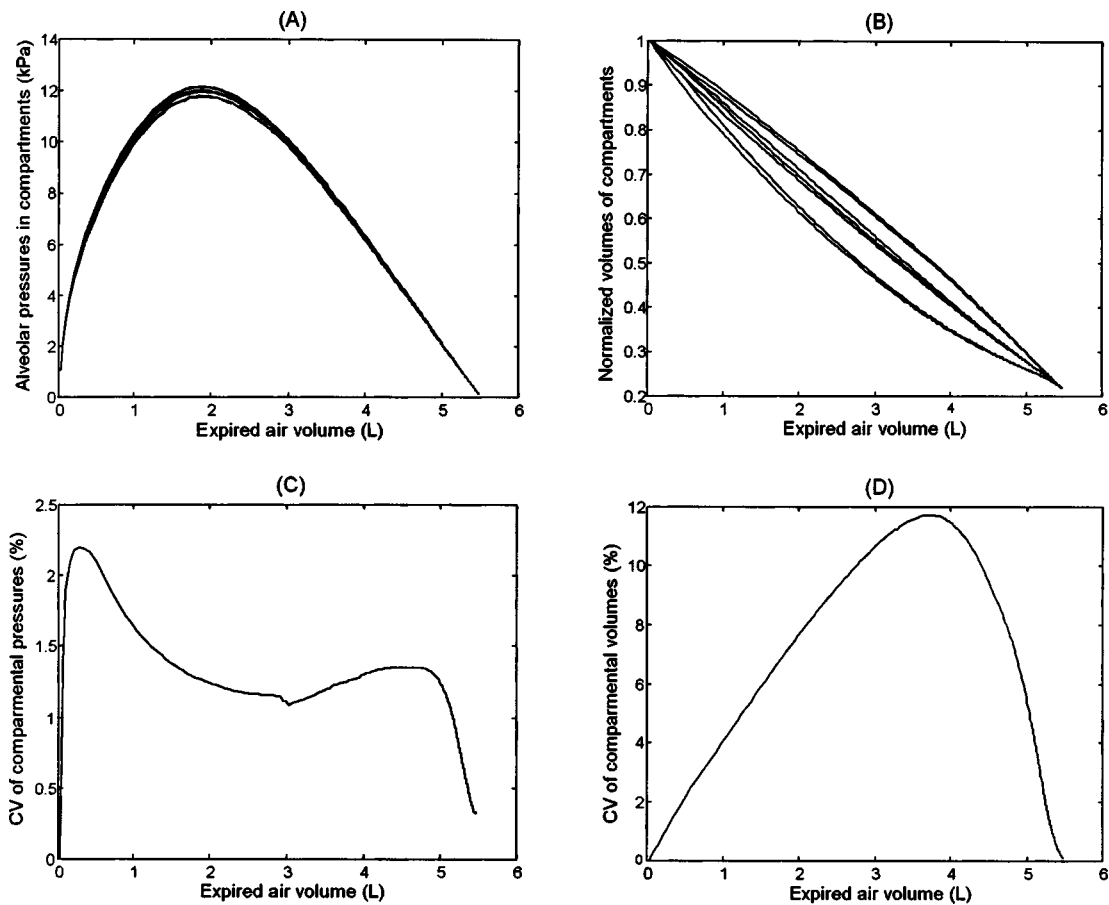


FIGURE 5. Nonuniform emptying of alveolar compartments: (A) alveolar pressures, (B) compartment volumes (normalized to their initial values), (C) coefficients of variation (CV) of pressure, and (D) CV of volume.

We also assumed there was a common static pressure at the downstream ends of daughter airways. The validity of this assumption can be assessed by comparison to the experimental data of Wilson *et al.*<sup>64</sup> Specifically, consider

the case of stiff symmetric tubes (lengths of 5.6 cm, cross-sectional areas ( $A_D$ ) of 1.27 cm<sup>2</sup>) connected to a mother one [length of 11.8 cm, cross-sectional area ( $A_M$ ) of 1.98 cm<sup>2</sup>], fed from two reservoirs with unequal pres-

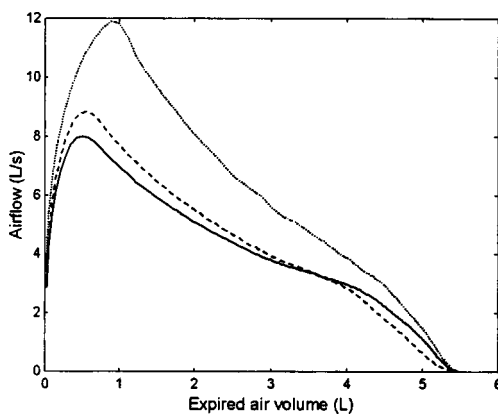


FIGURE 6. Influence of flow regime on maximal expiration: dissipative loss of pressure according to Reynolds (Ref. 46) (—), Reynolds and Lee (Ref. 47) (---), and Collins *et al.* (Ref. 8) (.....).

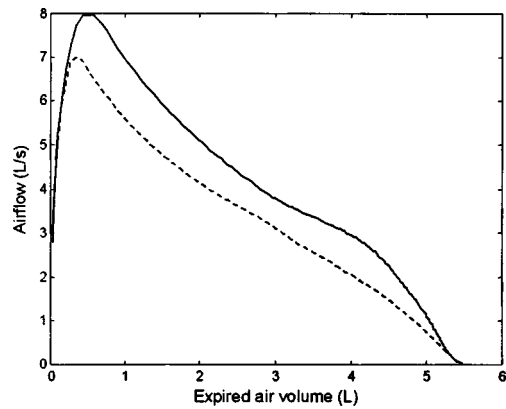


FIGURE 7. Maximum expiratory flow-volume curves calculated for the same structure of the bronchial tree using airway data published by Horsfield (—) and Weibel (---). Transformation between asymmetric and symmetric geometries presented in Table 1.

sures  $P_{01}$  and  $P_{02}$ , respectively. Conservation of energy at the junction yields the first governing equation:

$$\left( \frac{\rho q^2}{2A_M^2} + \Delta P_f(q) \right) q = [P_{01} - \Delta P_{f1}(q_1)] q_1 + [P_{02} - \Delta P_{f2}(q_2)] q_2, \quad (12)$$

where  $q$ ,  $q_1$ , and  $q_2$  are flows ( $q = q_1 + q_2$ ), and  $\Delta P_f$ ,  $\Delta P_{f1}$ , and  $\Delta P_{f2}$  are viscous pressure losses in the mother and daughter tubes, respectively [note that while Eq. (12) of this example was not used in the model for forced expiration it necessarily compliments Eq. (13) in solving the problem with two unknowns:  $q_1$  and  $q_2$ ]. Static pressure outside the downstream end of the mother tube is zero. Since the tube is uniform and flow is incompressible, the dynamic component is unchanged, but the static pressure (as well as total head) at the upstream end is larger by viscous dissipation ( $\Delta P_f$ ) along the mother tube. This implies that the sum in the brackets on the left side of Eq. (12) is a total head at the upstream end of the mother tube. Expressions in brackets on the right side of the equation describe the total heads at the downstream ends of the daughter tubes. The dissipative pressure drops are calculated with the empirical formula [Eq. (6)] for pressure–flow relationship in a single bifurcation. The second equation needed imposes equal static pressures of daughter tubes at their junction:

$$P_{01} - \Delta P_{f1}(q_1) - \frac{\rho q_1^2}{2A_D^2} = P_{02} - \Delta P_{f2}(q_2) - \frac{\rho q_2^2}{2A_D^2}. \quad (13)$$

We use this simplification though a transient region exists between the beginning of a mother airway and a point somewhere downstream, where the two “daughter streams” are “jointed” with straight and parallel streamlines. From the very beginning of the tube, however, the two streams are in lateral contact, and this is the direction in which the static pressure, not dynamic component, plays a crucial role. A potential difference between static pressures of the streams must lead to a quick radial shift of gas streamlines and the static pressure becomes uniform. Because we analyze an incompressible fluid, compensation of static pressure in a near distance from the merger must react on the streams in the downstream ends of the daughter tubes. Solving the system of two nonlinear Eqs. (12) and (13) with two unknowns ( $q_1$  and  $q_2$ ) with the Raphson–Newton numerical method<sup>43</sup> results in the simulations of Fig. 8 which are compared to the experimental data of Wilson *et al.*<sup>64</sup> Their empirical results and our simulation outcomes are highly consistent suggesting that the assumption of a common static pres-

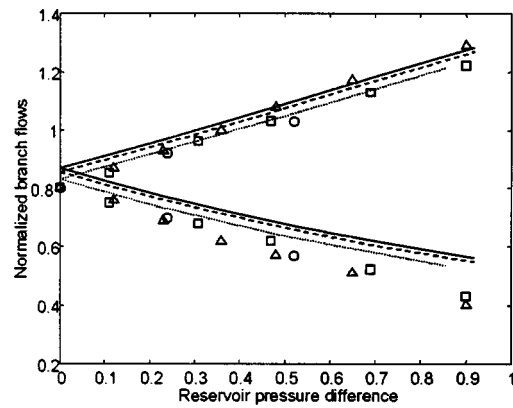


FIGURE 8. Comparison of experimental data of Wilson *et al.* (Ref. 64) (points) and the derived formula (lines) assuming common static pressure at the downstream ends of the daughter airways. Branch flows normalized to the maximal value of  $A_M/2\sqrt{2P_0/\rho}$ ,  $P_0 = (P_{01} + P_{02})/2$ , pressure difference given by  $(P_{01} - P_{02})/P_0$ .  $P_{01} = 1.3$  cm H<sub>2</sub>O (circles and dotted lines),  $P_{01} = 2.7$  cm H<sub>2</sub>O (squares and dashed lines), and  $P_{01} = 4.0$  cm H<sub>2</sub>O (triangles and solid lines).

sure at the downstream ends of the daughters is reasonable, at least in the above case.

#### Local Flow Limitation

During flow through an elastic tube there exists a wave speed of pressure disturbance propagation along the wall which influences the lateral pressure drop and controls airway collapsing.<sup>9,50</sup> The ratio between the local flow speed and wave speed, called the speed index ( $S$ ), varies along the tube. There is a possibility of two phenomena with regard to the speed index: choking of flow ( $S = 1$ ) and continuous passage through  $S = 1$  from sub- to supercritical values, both broadly described by Shapiro.<sup>50</sup> Transition to supercritical conditions typically results in shock-like waves. However, in a bronchial tree represented as a continuously branching symmetric network with a continuous variation of the total cross-sectional area (the “trumpet model”), there must be a smooth transition from subcritical to supercritical flow. Otherwise the speed index would equal unity in the mouth outlet during flow limitation.<sup>12</sup> In papers utilizing this model the speed index is allowed to exceed unity, and the boundary conditions are reached by placing an elastic jump downstream to the point of transition.<sup>10,12,51</sup> On the contrary, when each airway is treated as a uniform tube with unvarying physical properties, pure-friction flow may be the mechanism of airway collapsing [Eq. (4)], and in this instance  $S$  must go toward unity at the tube outlet (flow choking), and cannot pass through it.<sup>50</sup> The same mechanism subsists for more physiological context of vertical subjects, when the tubes slope upward (combined friction and gravity).<sup>50</sup> Such conditions are taken into account in the present work, keeping

in mind that before flow reaches the exact value of the wave speed, the lateral pressure drop in the tube may achieve any level [compare Eq. (4)], particularly the driving value. Our approach is consistent with some other works.<sup>26,27,28,42</sup>

Simulations with increased expiratory pressure (Fig. 4) have indicated moments when flows become independent of patient's effort, i.e., when flow limitation starts in individual branches. This phenomenon is accompanied by flow equalizing in compartments 1 and 6, 3 and 5, and 4 and 7. The reason is that the relevant airway branches are almost the same, except for the downstream parts (compare Fig. 1). Because airflow does not depend on the resistance downstream to the flow-limiting segment,<sup>35,44</sup> when the choke point is placed, e.g., in order 32 airways ( $A_6$  and  $A_5$ ), flows  $q_1$  and  $q_6$ , as well as  $q_4$  and  $q_7$ , should be the same for the same compartment volumes. Analogous are also flows  $q_3$  and  $q_5$ . The slight differences are caused by a distinct volume history of the alveolar regions—during the first part of unlimited flows the analogous compartments empty proportionally to the resistance of the whole airway branch leading to the mouth, so their volumes change nonuniformly. Thus, for a given total volume of expired air (abscissa in Fig. 4), they have somewhat different volumes (setting recoil pressures) and maximal flows. In other words, the local flows depend on upstream resistances and regional recoils, i.e., they are governed by local emptying time constants upstream from the choke points. Additionally, this implies that flows which were faster at the beginning of expiration (and decreased compartment volumes more rapidly), must be slower during flow limitation, as it can be seen in Fig. 4.

#### *Role of the Bronchial Tree Asymmetry*

The computational model enables choosing the order of airways, upstream of which the bronchial segments are symmetric. Thus, the smaller order selected, the more asymmetric structure of the bronchial tree. The effect of the heterogeneity level on the MEFV curve is irregular (see Fig. 3). First, changing the structure from the two-branch system (35th order selected, Fig. 1) to the three-branch one (order 34) increases airflow in the whole range of vital capacity. Then, on the contrary, choosing the 33rd order reduces airflow, just to enlarge it a little again for the 32nd order, etc. The reason lies in dimensions of the separate airways that appear during expansion of the structure. For example in case of 35th order selected, the left part of symmetric airways begins with  $A_2$  bronchus bifurcating into two airways of order 32 (Fig. 1, Table 1), whereas in case of selecting order 34, the same bronchus divides into airway orders 33 and 31. Since the ratios between the cross-sectional areas and lengths of the order 33 and 32 bronchi are about two

(Table 1, Horsfield's data), laminar flow increases also about two times, affecting the overall airflow. Now  $A_4$  and  $A_3$  bronchi are connected with airways of order 32 (symmetric subtrees). In the next step (order 33 chosen) both of them separate to order 32 and 29 bronchi, which must suppress the airflow. Moreover, the conditions of flow limitation, appearing first in the large airways and moving upstream during expiration, are also changed. Generally, upstream displacement of the asymmetry/symmetry margin suppresses the entire airflow, lowers the differences between the succeeding MEFV curves with a tendency to restrict them to smaller lung volumes. This implies that central heterogeneity of the bronchial tree plays a dominant role in constituting the shape of flow-volume curves. Based on a sensitivity analysis of a symmetric model, Lambert also concluded that central airway properties are a main factor determining maximal expiration, and the phenomena in peripheral airways influence only the last part of the MEFV curve.<sup>27</sup>

The development of choke points inside subtrees differs in an asymmetric structure. The case of flow limitation inside the subtrees is a parallel process (as in symmetric models). Nevertheless, the expiration simulated stays heterogeneous because each subtree generally varies from each other and the choke points may exist in different airway generations at any given moment.

The above results were achieved using the transition from the Weibel to Horsfield geometries as described in Preliminaries and given in Table 1. The increase in the asymmetry results in a variation in the total number of airways. It follows that different quantitative outcomes may be expected with another definition of mapping between Weibel's and Horsfield's models.

#### *Heterogeneous Lung Emptying*

Inhomogeneity of airway branches leading from the separate alveolar regions modulates individual airflows. Larger flows from compartments 1, 2, and 6, comparing with 3, 4, 5, and 7 (Fig. 4) results from the bigger dimensions of these lung regions. On the base of their experiments Warner *et al.*<sup>60</sup> postulated that each lung region possesses its own flow-volume curve. Two individual curves of distinct regions were presented *in vivo* by Mink<sup>38</sup> and simulated by Solway *et al.*<sup>52</sup> and Lambert.<sup>26</sup> Results of simulations for any level of asymmetry of our model, e.g., those shown in Fig. 4, prove that every distinct part of lungs is characterized by its own flow-volume relationship.

It has been demonstrated that even when there is a substantial inhomogeneity between two branches leading to the same parent airway, large differences between alveolar pressures are prevented.<sup>32,38,52,59,64</sup> Effects of the above mechanism are visible in Fig. 5. Differences in compartmental volumes are easily visible [Fig. 5(B)],

whereas alveolar pressures stay similar [Fig. 5(A)]. The reason stems from the fact that alternation of regional volumes modifies compartment recoils, which are the secondary components of compartmental pressures. The primary component of compartmental pressures is the pleural pressure which is the same for all lung regions. The volume trajectories [Fig. 5(B)] form an “onion skin,” observed during clinical experiments.<sup>33,37,65</sup> Since the simulations have been performed with uniform pleural pressure, it follows that the bronchial tree asymmetry is responsible for nongravitational variability of regional volumes.

Most of empirical studies on heterogeneous lung emptying were carried out with forced deflation<sup>16,32,38,56,59,60</sup> rather than subject initiated forced exhalation. With forced deflation trajectories of regional alveolar pressures descend in an exponential manner, whereas in forced expiration regional pressures must start from zero at the beginning, reach maximal values in the middle and fall to zero at the end of expiration [Fig. 5(A)]. Nevertheless, measured and calculated indices of heterogeneity can be analyzed. Topulos *et al.*<sup>56</sup> and Warner *et al.*<sup>59</sup> have shown that the standard deviation (SD) of regional pressures increases rapidly at the beginning of deflation, tends to decrease slightly over early deflation, and then increases somewhat before a final decrease at end of expiration. Their results are consistent with the calculated variation of the pressure CV presented in Fig. 5(C). Warner and co-workers<sup>60</sup> have also plotted the SD of regional volumes. They showed that inhomogeneities grow systematically until low lung volumes and then decrease rapidly. The same can be observed in the course of the regional volume CV shown in Fig. 5(D).

The shapes of CV curves are determined by the mean pressure and volume changes, the limitations in pressure differences between alveolar regions,<sup>56,64</sup> and the compartment volume–elastic recoil pressure relationships. First, nonuniform emptying of alveolar regions introduces rising differences in compartment volumes. Since lung elastance is large near TLC, differences in alveolar pressures grow even more rapidly. Then, flow limitation is established which keeps the rate of volume diverging. Alternatively, compartments containing higher pressures show a faster decrease of volume caused by faster airflows and this reduces compartment elastic recoils. The two aforementioned mechanisms are involved in the independence of regional expiratory flows.<sup>32,38,52,56,64</sup> The result is that their alveolar pressures are more uniform. Simultaneously mean  $P_A$  reaches maximal values, additionally suppressing the relevant CV. Coming to the end of expiration, the lungs become more compliant, amplifying differences of pressure in relation to regional volumes. Simultaneously the normalized volumes become very similar because the compartments which emptied quicker at the beginning now possess smaller recoil pres-

ures and generate smaller airflows (and *vice versa*), as found also by Mink.<sup>38</sup> This explains why smaller volumes empty slower while the bigger ones empty faster.

Variation of compartmental volumes may cause local deviations in pleural pressure while simultaneously modifying compartmental pressures. Hence, regional transmural pressures stay unchanged [compare Eq. (2)]. It follows that compartmental flows are independent on this phenomenon during flow limitation.

#### *Importance of the Physiological Data Used*

One of the factors determining transmural pressure in an airway, and thus its caliber, is dissipative pressure loss between the alveoli and a bronchus. The empirical formulas used in our simulations (Fig. 6) differ in the amount of this pressure loss. Changing coefficient values in Eq. (5) from  $a=1.5$  and  $b=0.0035$  (applied as basic in the computational model) to  $a=3.4$  and  $b=0.0021$  increases the ratio between laminar and turbulent factors. This enlarges the airflow at the beginning of expiration, since it is constituted by the central airways with prevailing turbulent flow, which now entails smaller head pressure losses. On the contrary, the last part of the MEFV curve is controlled by the peripheral airways. Because laminar flow predominates in them and the laminar part of dissipation is magnified, flow is smaller. Using the Collins Eq. (6) instead of the Reynolds one, introduces smaller pressure loss for any flow<sup>8</sup> and the maximal airflow is systematically increased. The differences between the simulated curves in Fig. 6 do not question the usefulness of the model investigations on effects of structural asymmetries on MEFV curves when using a particular description for dissipative pressure loss. Rather, the results of Fig. 6 provide an insight how the relation of laminar versus turbulent flows might alter the results. This issue has concerned all previous approaches of mathematical modeling of forced expiration. Our model allows it to be explored in a more robust fashion relative to airway branching structure. This remark applies also to the use of particular morphometric data, discussed next.

Prediction of the MEFV curve with the asymmetric structure of the bronchial tree and Weibel's dimensions of airways instead of Horsfield's ones creates systematically lower flows in the whole range of vital capacity. Direct comparison of airway areas (Table 1) indicates that Weibel's trachea and main bronchi are larger than Horsfield's ones, whereas airways of generations from 3 to 12 are smaller. Since the choke points appear in large bronchi and move upstream during expiration, maximal flow is controlled by these airway dimensions, and the size of downstream bronchi does not play a crucial role. Moreover, the central airways are the main site of dissipative pressure losses. Thus, smaller cross-sectional areas

given by Weibel seem to be the main source of airflow suppression. Even if small airways in acini region have bigger areas in Weibel data, their contribution to the upstream resistance is negligible comparing with bigger bronchioli, and cannot alter the effect caused by the central airways.

## CONCLUSIONS

We have advanced a computational model enabling simulation of forced expiration from multi-compartment lungs through the asymmetric, Horsfield-based structure of the bronchial tree. It extends previous approaches that have been limited usually to two alveolar regions and meets the need of a tool for analysis of complex, nonlinear phenomena proceeding in the respiratory system during maximum expiration. This maneuver is a standard test for lung function examination. Hence, detailed insight on how structural features of the airway tree, including its inherent asymmetry, impact maximum expiration are essential to fully understand the relation between lung mechanics and shapes of the MEFV curves, especially during heterogeneous lung disease.

Simulations performed show that the model captures the main phenomena observed *in vivo* during forced expiration: effort independence of the flow–volume curve for most of vital capacity, independence of limited flow on the properties of airways downstream to a choke point, characteristic differences of lung regional pressures and volumes, and a shape of their variability during exhalation. The analysis done also demonstrates the importance of a proper mathematical description of viscous pressure losses in the bifurcating system of airways as well as of the form of airway area–transmural pressure relationships. The dependencies used in the present study are based on old empirical records and their extrapolations. New, more precise data would improve the accuracy of the computational model.

Some new insights into flow limitation mechanism and inhomogeneous lung emptying were achieved as a result of this study. First, flow limitation begins at slightly different time instants in individual branches of the bronchial tree, however after a short period of time, all regional flows are limited in a parallel fashion. Hence, total flow at the mouth is limited for most of the expired lung volume. Second, each of the airway branches posses their own flow–volume shape and just these individual flows constitute the measured MEFV curve. Third, central airway heterogeneity can play a crucial role in modification of the entire flow. Fourth, the bronchial tree asymmetry is responsible for a nongravitational component of regional volume variability. Finally, increased inhomogeneity yields results that cannot be explained nor re-created with the use of a symmetrical structure of the bronchial tree.

## ACKNOWLEDGMENTS

This work was supported by Nos. NSF-BES-0076818 and NIH HL62269-03. One of the authors was also supported in part by Grant No. 8 T10C 025 21 from the State Committee for Scientific Research (Poland).

## APPENDIX: ALGORITHM DETAILS

To find compartmental airflows matching pressure losses and driving pressures at the airway branches the system of Eqs. (9) must be solved. Solving a set of nonlinear equations is probably more art than engineering and getting to success depends on *a priori* knowledge on the behavior of the equations, since there are no general methods for solving systems of more than one equation. The iterative Raphson–Newton method has been selected, requiring calculation of the Jacobian matrix ( $\mathbf{J}$ ) (Ref. 43) of a reorganized set of equations.

Rewriting Eq. (9) in the following form:

$$\begin{aligned} h_1(q_1, q_2, \dots, q_k) &= 0, \\ h_2(q_1, q_2, \dots, q_k) &= 0, \\ &\vdots \\ h_k(q_1, q_2, \dots, q_k) &= 0, \end{aligned} \quad (\text{A1})$$

where  $h_i(q_1, q_2, \dots, q_k) = \sum_i \Delta P_i(q_1, q_2, \dots, q_k) - P_{dj}$ , indicates the formulas used for the calculation of the Jacobian

$$J(i, j) \equiv \frac{\partial h_i}{\partial q_j}. \quad (\text{A2})$$

Then, a small incrementation of flow vector ( $\Delta \mathbf{q}$ ) in each iteration step is given:

$$\Delta \mathbf{q} = -\mathbf{J}^{-1} \mathbf{h}(\mathbf{q}), \quad (\text{A3})$$

where  $\mathbf{q} = [q_1, q_2, \dots, q_k]^T$  and  $\mathbf{h} = [h_1, h_2, \dots, h_k]^T$  are vectors of flows  $q$  and functions  $h$ , respectively.

Since functions  $h$  are sums of pressure drops along appropriate airways, derivatives of  $h$  on  $q$  are sums of these pressure loss derivatives on flows. Moreover, it is important to notice that each pressure drop depends also on transmural pressure at the beginning (upstream end) of a bronchus ( $P_{tm0}$ ), controlling airway inlet caliber. Then,

$$\frac{d\Delta P}{dq} = \left( \frac{\partial \Delta P}{\partial q} \right)_{P_{tm0}} + \left( \frac{\partial \Delta P}{\partial P_{tm0}} \right) \frac{dP_{tm0}}{dq}. \quad (\text{A4})$$

To calculate derivative of pressure drop on flow for the given value of  $P_{tm0}$ , Eq. (4) must be used:

$$\frac{\partial \Delta P}{\partial q} = \int_0^l \frac{\partial^2 P}{\partial x \partial q} dx. \quad (\text{A5})$$

Pressure drop derivative on  $P_{tm0}$  for the given flow value may be rewritten as follows:

$$\frac{\partial \Delta P}{\partial P_{tm0}} = \int_0^l \frac{\partial^2 P(x)}{\partial x \partial P_{tm0}} dx = \int_0^l \frac{\partial^2 P(x)}{\partial x \partial A(x)} \left( \frac{\partial A}{\partial P_{tm}} \right) \frac{\partial P_{tm}(x)}{\partial P_{tm0}} dx, \quad (\text{A6})$$

and additionally,

$$\frac{\partial P_{tm}(x)}{\partial P_{tm0}} = 1 - \frac{\partial \Delta P(x)}{\partial P_{tm0}}, \quad (\text{A7})$$

since transbronchial pressure at the point  $x$  in the airway

$$P_{tm}(x) = P_{tm0} - \Delta P(x). \quad (\text{A8})$$

Substituting Eqs. (A7) into (A6) gives

$$\frac{\partial \Delta P}{\partial P_{tm0}} = \int_0^l \frac{\partial^2 P(x)}{\partial x \partial A(x)} \left( \frac{\partial A}{\partial P_{tm}} \right) \left( 1 - \frac{\partial \Delta P(x)}{\partial P_{tm0}} \right) dx. \quad (\text{A9})$$

Note that the exact calculation of the influence of  $P_{tm0}$  on  $\Delta P$  along an airway needs solving one more differential equation. To avoid additional computational time, the linear extrapolation of  $\partial \Delta P(x)/\partial P_{tm0}$  is used during the integration. Transmural pressure  $P_{tm0}$  is given by the difference between recoil pressure of the alveolar compartment and static pressure drop along connecting airways, i.e., the sum of pressure losses in the succeeding bronchi:

$$P_{tm0} = P_{st}(V_C) - \sum_i \Delta P_i, \quad (\text{A10})$$

and then

$$\frac{dP_{tm0}}{dq} = - \sum_i \frac{d\Delta P_i}{dq}. \quad (\text{A11})$$

Hence, to evaluate this dependence, pressure loss derivatives on flow of more peripheral airways must be known. In fact they are known [see Eq. (A4)], since calculations start from the most peripheral airways and are continued downstream to the upper airways.

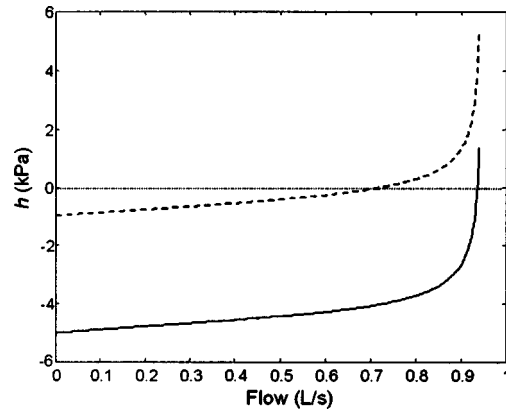


**FIGURE A1.** Dependence of function  $h$  on flow through an airway of 32nd order for a one compartmental lung model: the airway connected with an alveolar compartment by a linear resistance of 1 kPa/(L/s), compartmental recoil pressure of 0.5 Pa, driving pressure of 1 (---) and 5 (—) kPa, zeros of  $h$  at flows about 0.730 and 0.936 L/s, respectively.

Integration of the differential Eq. (4) is done with the fourth- and fifth-order Runge–Kutta method<sup>43</sup> and other integrations use Newton–Cotes (trapezoidal) rule<sup>43</sup> at points yield by the Runge–Kutta procedure. Numerical integration of the lateral pressure for the giving flow proceeds in the downstream direction for the intrathoracic airways (initial condition set by the pressure loss in the more peripheral bronchi and the acting pleural pressure) and in the opposite direction for the trachea (initial condition specified by pressure drop in the upper airways). Since the multistep methods for solving differential equations apply small increments of integrated quantity to assess the solution and its accuracy in each step, flow could shift from sub- to supercritical value inside such a procedure, despite physical restrictions. Thus, the condition of submaximal flows is kept by additional control of Runge–Kutta procedure. Modifications of the lateral pressure in the airway junctions are neglected.

Functions  $h(\mathbf{q})$  are singular for the flow values resulting in the wave speed in any airway belonging to the pathway (Fig. A1) and are treated as having no values for higher flows. Thus, according to the Lambert equation, flow cannot exceed the wave speed (for details see the Discussion). The Newton–Raphson method used in this work for solving the system of nonlinear equations (i.e., finding zeros of  $\mathbf{h}$ ) involves calculations of derivatives of these functions on flows to find next approximation of flow values in the iterative procedure. It may happen, however, especially for higher driving pressures (see Fig. A1), that the flow searched is very close to the wave speed and the step of the Newton–Raphson routine yields a value higher than the critical flow. To be able to find appropriate flows, at every lung volume calculations start with small values ensuring the possibility of com-

puting flow increments, according to Eq. (A3), at least at the first step (see Fig. 2). When flow limitation is deduced, last increments of flows coming to the flow-limiting airway are reduced by half, and calculations are repeated until non-limiting flows are achieved or the criteria that brake the loop are reached. It is worthy to mention that good resolution in flow can be achieved with simultaneous poor resolution of pressure drop, since very small deviation in flow close to wave speed produces big variation in pressure loss.

Too small airflow in one of iterations can produce too small pressure drop and in the next step this airflow will be increased, potentially yielding too large pressure drop. This can cause the procedure to be not convergent. To improve convergence of the algorithm, a few constraints on flow increments have been imposed.

The condition that differences between recoil pressures of alveolar compartments and pressure drops along pathways leading from them to the given airway are equal must be satisfied during airflow through the bronchial tree, since these differences represent the same transmural pressure at the airway junction. During iterative calculations, however, it need not be the case, since actual flows differ from the final values. To improve accuracy of computations, an additional constraint has been imposed on flow increments in case of flow limitation: the change of total flow through the airway must be not only half the previous one, but also changes of flows coming into this airway from the daughter ones should guarantee the same value of  $P_{tm0}$ . Sensitivities of pressure losses on these two airflows, known at this point, are used to this goal.

### NOMENCLATURE

$A$	cross-sectional area of an airway
$C_E$	lung compliance at zero recoil pressure
$f$	elementary dissipative pressure loss
$l_{RV}$	airway length at residual volume
$N_{alv}$	total number of alveoli
$N_{ak}$	number of alveoli in the $k$ th compartment
$P$	lateral pressure to the airway wall
$P_A$	alveolar pressure
$P_d$	driving pressure
$P_m$	maximal expiratory pressure
$P_{pl}$	pleural pressure
$P_{st}$	static recoil pressure of a lung
$P_{tm}$	transmural pressure
$P_{tm0}$	transmural pressure at the upstream end of an airway
$Q$	total airflow measured in the mouth
$q$	local airflow
RV	residual volume
$R_N$	Reynolds number
$R_T$	thorax tissue resistance

$S$	speed index
$t$	time
VC	vital capacity
$V_0$	minimal lung volume
$V_{Ck}$	volume of the $k$ th alveolar compartment
$V_L$	lung volume
$V_m$	maximal lung volume
$V_t$	lung tissue volume
$V_{tr}$	transition volume
$x$	a point inside an airway
$\Delta P$	lateral pressure drop along an airway
$\Delta P_{it}$	lateral pressure drop between alveoli and a given point
$\mu$	gas viscosity
$\rho$	gas density
$\tau$	time constant of expiratory muscle

### REFERENCES

- Agostoni, E., and W. O. Fenn. Velocity of muscle shortening as a limiting factor in respiratory air flow. *J. Appl. Physiol.* 15:349–353, 1960.
- Anafi, R. C., and T. A. Wilson. Airway stability and heterogeneity in the constricted lung. *J. Appl. Physiol.* 91:1185–1192, 2001.
- Barnea, O., S. Abboud, A. Guber, and I. Bruderman. New model-based indices for maximum expiratory flow–volume curve in patients with chronic obstructive pulmonary disease. *Comput. Biol. Med.* 26:123–131, 1996.
- Bloch, K. E., C. L. Georgescu, E. W. Russi, and W. Weder. Gain and subsequent loss of lung function after lung volume reduction surgery in cases of severe emphysema with different morphologic patterns. *J. Thorac. Cardiovasc. Surg.* 123:845–854, 2002.
- Bogaard, J. M., S. E. Overbeek, A. F. M. Verbraak, C. Vons, H. T. M. Folgering, Th. W. van der Mark, C. M. Roos, P. J. Sterk, and the Dutch CNSLD study group. Pressure–volume analysis of the lung with an exponential and linear-exponential model in asthma and COPD. *Eur. Respir. J.* 8:1525–1531, 1995.
- Cederlund, K., U. Tylene, L. Jorfeldt, and P. Aspelin. Classification of emphysema in candidates for lung volume reduction surgery (\*): A new objective and surgically oriented model for describing CT severity and heterogeneity. *Chest* 122:590–596, 2002.
- Colebatch, H. J. H., C. K. Y. Ng, and N. Nikov. Use of an exponential function for elastic recoil. *J. Appl. Physiol.: Respir., Environ. Exercise Physiol.* 46:387–393, 1979.
- Collins, J. M., A. H. Shapiro, E. Kimmel, and R. D. Kamm. The steady expiratory pressure–flow relation in a model pulmonary bifurcation. *J. Biomech. Eng.* 115:299–305, 1993.
- Dawson, S. D., and E. A. Elliott. Wave-speed limitation on expiratory flow—A unifying concept. *J. Appl. Physiol.: Respir., Environ. Exercise Physiol.* 43:498–515, 1977.
- Elad, D., and R. D. Kamm. Parametric evaluation of forced expiration using a numerical model. *J. Biomech. Eng.* 111:192–199, 1989.

- <sup>11</sup>Elad, D., R. D. Kamm, and A. H. Shapiro. Tube law for the intrapulmonary airway. *J. Appl. Physiol.* 65:7–13, 1988.
- <sup>12</sup>Elad, D., R. D. Kamm, and A. H. Shapiro. Mathematical simulation of forced expiration. *J. Appl. Physiol.* 65:14–25, 1988.
- <sup>13</sup>Fredberg, J. J., and D. Stamenovic. On the imperfect elasticity of lung tissue. *J. Appl. Physiol.* 67:2408–2419, 1989.
- <sup>14</sup>Fry, D. L. A preliminary lung model for simulating the aerodynamics of the bronchial tree. *Comput. Biomed. Res.* 2:111–134, 1968.
- <sup>15</sup>Fry, D. L., R. V. Ebert, W. W. Stead, and C. C. Brown. The mechanics of pulmonary ventilation in normal subjects and in patients with emphysema. *Am. J. Med.* 16:80–97, 1954.
- <sup>16</sup>Georgopoulos, D., A. Gomez, and S. N. Mink. Factors determining lobar emptying during maximal and partial forced deflations in nonhomogeneous airway obstruction in dogs. *Am. J. Respir. Crit. Care Med.* 149:1241–1247, 1994.
- <sup>17</sup>Georgopoulos, D., S. N. Mink, L. Oppenheimer, and N. R. Anthonisen. How is maximal expiratory flow reduced in canine postpneumectomy lung growth? *J. Appl. Physiol.* 71:834–840, 1991.
- <sup>18</sup>Gillis, H. L., and K. R. Lutchen. How heterogeneous bronchoconstriction affects ventilation distribution in human lungs: a morphometric model. *Ann. Biomed. Eng.* 27:14–22, 1999.
- <sup>19</sup>Gillis, H. L., and K. R. Lutchen. Airway remodeling in asthma amplifies heterogeneities in smooth muscle shortening causing hyperresponsiveness. *J. Appl. Physiol.* 86:2001–2012, 1999.
- <sup>20</sup>Hammersley, J. R., and D. E. Olson. Physical model of the smaller pulmonary airways. *J. Appl. Physiol.* 72:2402–2414, 1992.
- <sup>21</sup>Horsfield, K., G. Dart, D. E. Olson, and G. Cumming. Models of the human bronchial tree. *J. Appl. Physiol.* 31:207–217, 1971.
- <sup>22</sup>Hughes, J. M. B., F. G. Hoppin, Jr., and J. Mead. Effect of lung inflation on bronchial length and diameter in excised lungs. *J. Appl. Physiol.* 32:25–35, 1972.
- <sup>23</sup>Hyatt, R. E. Expiratory flow limitation. *J. Appl. Physiol.: Respir., Environ. Exercise Physiol.* 55:1–8, 1983.
- <sup>24</sup>Hyatt, R. E., D. P. Schilder, and D. L. Fry. Relationship between maximum expiratory flow and degree of lung inflation. *J. Appl. Physiol.* 13:331–336, 1958.
- <sup>25</sup>Jaeger, M. J., and H. Matthys. The pattern of flow in the upper human airways. *Respir. Physiol.* 6:113–127, 1969.
- <sup>26</sup>Lambert, R. K. A new computational model for expiratory flow from nonhomogeneous human lungs. *J. Biomech. Eng.* 111:200–205, 1989.
- <sup>27</sup>Lambert, R. K. Sensitivity and specificity of the computational model for maximal expiratory flow. *J. Appl. Physiol.: Respir., Environ. Exercise Physiol.* 57:958–970, 1984.
- <sup>28</sup>Lambert, R. K., T. A. Wilson, R. E. Hyatt, and J. R. Rodarte. A computational model for expiratory flow. *J. Appl. Physiol.: Respir., Environ. Exercise Physiol.* 52:44–56, 1982.
- <sup>29</sup>Landau, L. I., L. M. Taussig, P. T. Macklem, and P. H. Beaudry. Contribution of inhomogeneity of lung units to the maximal expiratory flow–volume curve in children with asthma and cystic fibrosis. *Am. Rev. Respir. Dis.* 111:725–731, 1975.
- <sup>30</sup>Lutchen, K. R., J. L. Greenstein, and B. Suki. How inhomogeneities and airway walls affect frequency dependence and separation of airway and tissue properties. *J. Appl. Physiol.* 80:1696–1707, 1996.
- <sup>31</sup>Lutchen, K. R., A. Jensen, H. Atileh, D. W. Kaczka, E. Israel, B. Suki, and E. P. Ingenito. Airway constriction pattern is a central component of asthma severity. *Am. J. Respir. Crit. Care Med.* 164:207–215, 2001.
- <sup>32</sup>McNamara, J. J., R. G. Castile, G. M. Glass, and J. J. Fredberg. Heterogeneous lung emptying during forced expiration. *J. Appl. Physiol.* 63:1648–1657, 1987.
- <sup>33</sup>McNamara, J. J., R. G. Castile, M. S. Ludwig, G. M. Glass, R. H. Ingram, Jr., and J. J. Fredberg. Heterogeneous regional behavior during forced expiration before and after histamine inhalation in dogs. *J. Appl. Physiol.* 76:356–360, 1994.
- <sup>34</sup>Mead, J. Analysis of the configuration of maximum expiratory flow–volume curves. *J. Appl. Physiol.: Respir., Environ. Exercise Physiol.* 44:156–165, 1978.
- <sup>35</sup>Mead, J., J. M. Turner, P. T. Macklem, and J. B. Little. Significance of the relationship between lung recoil pressure and maximum expiratory flow. *J. Appl. Physiol.* 22:95–108, 1967.
- <sup>36</sup>Melissinos, C. G., P. Webster, Y. K. Tien, and J. Mead. Time dependence of maximum flow as an index of nonuniform emptying. *J. Appl. Physiol.: Respir., Environ. Exercise Physiol.* 47:1043–1050, 1979.
- <sup>37</sup>Milic-Emili, J. J., A. M. Henderson, M. B. Dolovich, D. Trop, and K. Kaneko. Regional distribution of inspired gas in the lung. *J. Appl. Physiol.* 21:749–759, 1966.
- <sup>38</sup>Mink, S. N. Mechanism of lobar alveolar pressure decline during forced deflation in canine regional emphysema. *J. Appl. Physiol.* 82:632–643, 1997.
- <sup>39</sup>Mroccka, J., and A. G. Polak. Noninvasive method for measurement of respiratory system parameters. Proceedings of the XIII IMEKO World Congress, Torino, 5–9 September 1994, Vol. 2, pp. 1561–1565.
- <sup>40</sup>Pardaens, J., K. P. van de Woestijne, and J. Clément. A physical model for expiration. *J. Appl. Physiol.* 33:479–490, 1972.
- <sup>41</sup>Pardaens, J., K. P. van de Woestijne, and J. Clément. Simulation of regional lung emptying during slow and forced expirations. *J. Appl. Physiol.* 39:191–198, 1975.
- <sup>42</sup>Polak, A. G. A forward model for maximum expiration. *Comput. Biol. Med.* 28:613–625, 1998.
- <sup>43</sup>Press, W. H., B. P. Flannery, S. A. Teukolsky, and W. T. Vetterling. Numerical Recipes: The Art of Scientific Computing. Cambridge, MA: Cambridge University Press, 1986.
- <sup>44</sup>Pride, N. B., S. Permutt, R. L. Riley, and B. Bromberger-Barnea. Determinants of maximal expiratory flow from the lungs. *J. Appl. Physiol.* 23:646–662, 1967.
- <sup>45</sup>Renotte, C., M. Remy, and Ph. Saucez. Dynamic model of airway pressure drop. *Med. Biol. Eng. Comput.* 36:101–106, 1998.
- <sup>46</sup>Reynolds, D. B. Steady expiratory flow–pressure relationship of a model of the human bronchial tree. *J. Biomech. Eng.* 104:153–158, 1982.
- <sup>47</sup>Reynolds, D. B., and J.-S. Lee. Steady pressure–flow relationship of a model of the canine bronchial tree. *J. Appl. Physiol.: Respir., Environ. Exercise Physiol.* 51:1072–1079, 1981.
- <sup>48</sup>Robatto, F. M., S. Simard, and M. S. Ludwig. How changes in the serial distribution of bronchoconstriction affect lung mechanics. *J. Appl. Physiol.* 74:2838–2847, 1993.
- <sup>49</sup>Salazar, E., and J. H. Knowles. An analysis of pressure–volume characteristics of the lungs. *J. Appl. Physiol.* 19:97–104, 1964.
- <sup>50</sup>Shapiro, A. H. Steady flow in collapsible tubes. *J. Biomech. Eng.* 99:126–147, 1977.
- <sup>51</sup>Shin, J. J., D. Elad, and R. D. Kamm. Simulation of forced breathing maneuvers. In: Biological Flow, edited by M. Y. Jaffrin and C. Caro. New York: Plenum, 1995.
- <sup>52</sup>Solway, J., J. J. Fredberg, R. H. Ingram, Jr., O. F. Pedersen,

- and J. M. Drazen. Interdependent regional lung emptying during forced expiration: a transistor model. *J. Appl. Physiol.* 62:2013–1025, 1987.
- <sup>53</sup>Sud, V. K., R. Srinivasan, J. B. Charles, and M. W. Bungo. Effect of lower-body negative pressure on blood flow with applications to the human cardiovascular system. *Med. Biol. Eng. Comput.* 31:569–575, 1993.
- <sup>54</sup>Thorpe, C. W., and J. H. T. Bates. Effect of stochastic heterogeneity on lung impedance during acute bronchoconstriction: a model analysis. *J. Appl. Physiol.* 82:1616–1625, 1997.
- <sup>55</sup>Thurnheer, R., H. Engel, W. Weder, U. Stammberger, I. Laube, E. W. Russi, and K. E. Bloch. Role of lung perfusion scintigraphy in relation to chest computed tomography and pulmonary function in the evaluation of candidates for lung volume reduction surgery. *Am. J. Respir. Crit. Care Med.* 159:301–310, 1999.
- <sup>56</sup>Topulos, G. P., G. Nielan, G. Glass, and J. J. Fredberg. Interdependence of regional expiratory flows limits alveolar pressure differences. *J. Appl. Physiol.* 69:1413–1418, 1990.
- <sup>57</sup>Verbanck, S., D. Schuermans, A. Van Muylem, M. Noppen, and W. Vincken. Ventilation distribution during histamine provocation. *J. Appl. Physiol.* 83:1907–1916, 1997.
- <sup>58</sup>Verbanck, S., D. Schuermans, M. Noppen, W. Vincken, and M. Paiva. Methacholine versus histamine: paradoxical response of spirometry and ventilation distribution. *J. Appl. Physiol.* 91:2587–2594, 2001.
- <sup>59</sup>Warner, D. O., R. E. Hyatt, and K. Rehder. Inhomogeneity during deflation of excised canine lungs. I. Alveolar pressures. *J. Appl. Physiol.* 65:1757–1765, 1988.
- <sup>60</sup>Warner, D. O., R. E. Hyatt, and K. Rehder. Inhomogeneity during deflation of excised canine lungs. II. Alveolar volumes. *J. Appl. Physiol.* 65:1766–1774, 1988.
- <sup>61</sup>Weibel, E. R. *Morphometry of the Human Lung*. New York: Academic, 1963.
- <sup>62</sup>Wheatley, J. R., T. C. Amis, and L. A. Engel. Nasal and oral airway pressure–flow relationships. *J. Appl. Physiol.* 71:2317–2324, 1991.
- <sup>63</sup>Wiggs, B. R., R. Moreno, J. C. Hogg, C. Hilliam, and P. D. Paré. A model of the mechanics of airway narrowing. *J. Appl. Physiol.* 69:849–860, 1990.
- <sup>64</sup>Wilson, T. A., J. J. Fredberg, J. R. Rodarte, and R. E. Hyatt. Interdependence of regional expiratory flow. *J. Appl. Physiol.* 59:1924–1928, 1985.
- <sup>65</sup>Wilson, T. A., M. J. Hill, and R. D. Hubmayr. Regional lung volume trajectories during expiratory flow in dogs. *J. Appl. Physiol.* 80:1144–1148, 1996.